# Synthesis of $\alpha$-Fe$_2$O$_3$@SnO$_2$ core-shell nanoparticles via low-temperature molten salt reaction route

Gang LIU[1,2], Wei-jia SUN[2], Sha-sha TANG[3], Shu-quan LIANG[3], Jun LIU[3]

1. Department of Hepatobiliary & Enteric Surgery Research Center, Xiangya Hospital,
Central South University, Changsha 410008, China;
2. Department of General Surgery, Xiangya Hospital, Central South University, Changsha 410008, China;
3. School of Materials Science and Engineering, Central South University, Changsha 410083, China

**Abstract:** A cost-effective carbon-free nanocoating strategy was developed for the synthesis of ultra-fine SnO$_2$ coating $\alpha$-Fe$_2$O$_3$ core-shell nanoparticles. This strategy only involves a two-step molten salt reaction at low temperature of 300 °C. The as-prepared $\alpha$-Fe$_2$O$_3$@SnO$_2$ core-shell nanocomposites show enhanced electrochemical performances than the bare $\alpha$-Fe$_2$O$_3$ nanoparticles. This involved metal oxide nanocoating method is easy to be carried out, and the heat treatment temperature is much lower than that of other traditional solid-state annealing method and many carbon or metal oxide nanocoating methods. The molten salt method may also be used to produce other metal oxides coating nanostructures as the electrode materials for lithium-ion batteries.
**Key words:** nanometer materials; lithium-ion batteries; molten salt reaction; energy materials; nano-coating

## 1 Introduction

Lithium-ion batteries (LIBs) are the leading power source for portable electronic devices, which have been regarded as the promising power source of electric vehicles and hybrid electric vehicles [1]. Nowadays, carbon-based materials are the most widely commercialized anode materials. However, the low theoretical specific capacity (372 mA·h/g) and degraded cycling stability of carbon-based materials cannot fulfill the increasing demands for high performance LIBs. Large efforts have devoted into the study of replaceable anode materials [2,3]. Iron-based oxides ($\alpha$-Fe$_2$O$_3$) have attracted intensive research attention due to their higher theoretical specific capacity (1005 mA·h/g) [4]. However, the poor electrical conductivity and other drawbacks prevent the promotion of iron-based oxides.

Fe$_2$O$_3$ nanoparticles with electronically conductive coating layers appear to be more efficient for improving their electrochemical performances, due to better electrical conductivity and shorter transport length of both lithium ions and electrons. A successful example of the strategy is the well-known carbon-based coating technique, such as carbon-coated Fe$_2$O$_3$ composites [5,6]. In addition, carbon-free coating method, such as Mo$_2$N coating MoO$_2$ [2], Al$_2$O$_3$ coating LiCoO$_2$ [7], rutile TiO$_2$ coating Li$_4$Ti$_5$O$_{12}$ at 500 °C [8], SnO$_2$ coating $\alpha$-Fe$_2$O$_3$ by hydrothermal reaction [9], has been reported and shows enhanced performances. SnO$_2$, with high conductivity compared with other oxides, possesses a wide range of applications in photocatalysts, gas sensing and lithium-ion batteries (LIBs) [10,11]. SnO$_2$ as a coating layer on $\alpha$-Fe$_2$O$_3$ will benefit the performance of $\alpha$-Fe$_2$O$_3$/SnO$_2$, especially, heterostructures (HSs) of $\alpha$-Fe$_2$O$_3$/SnO$_2$ have demonstrated that it is an effective strategy to significantly improve their application performance. In most cases of the reported $\alpha$-Fe$_2$O$_3$/SnO$_2$ HSs, a hydrothermal or solvothermal method is usually employed based on the preferential growth of SnO$_2$ on different Fe$_2$O$_3$ seeds [12−14]. However, the involved coating or composing method is often complicated or at high reaction temperatures. It is an urgent need to investigate a cost-effective carbon-free

nanocoating strategy of advanced anode materials.

Herein, an effective carbon-free nanocoating strategy was developed to accomplish ultra-fine $SnO_2$ coating $\alpha$-$Fe_2O_3$ core-shell nanoparticles. This strategy only involves a two-step molten salt reaction (shown in Fig. 1). The selected eutectic mixed lithium salt system of LiCl and $LiNO_3$ has a relatively low melt point of about 300 °C, and it is helpful in preventing the growth of nanoparticles and controlling the particle morphology. The as-prepared $\alpha$-$Fe_2O_3$@$SnO_2$ core-shell nanoparticles show enhanced specific capacity and better electrical conductivity compared with those reported in Refs. [9,15]. This involved metal oxide nanocoating method is easy to be carried out and scaled up, and the heat treatment temperature is much lower than that of other traditional solid-state annealing method and other nanocoating methods, so it is economical and practical to realize the industrialization, and may also be used to produce other metal oxides coating nanostructures as electrode materials for LIBs.

## 2 Experimental

In a typical synthesis (Fig. 1), LiCl and $LiNO_3$ were mixed with iron (III) chloride hexahydrate in a mole ratio of 14:6:1, and 30 mL anhydrous ethanol was added into. After stirring for 10 min, the homogeneously mingled solution was dried at 80 °C, followed by a further heat-treatment at 300 °C for 3 h in a muffle furnace. After cooling down, the product was washed to remove the lithium salt and dried at 80 °C. Then, similar processes were performed according to the above steps to coat a layer of $SnO_2$ nanoparticles with mass fraction of 10%.

For electrochemical tests, CR 2016 coin cells were laboratory-assembled in a argon-filled glove box (Mbraun, Unilab, Germany), with Li metal as the reference electrode and 1 mol/L $LiPF_6$ dissolved in a mixture of ethylene carbonate/dimethyl carbonate/ethyl methyl carbonate (1:1:1, volume ratio) as the electrolyte. The working electrodes were prepared by mixing the active material with acetylene black and polyvinylidene fluoride at a mass ratio of 7:2:1 in N-methyl-2-pyrrolidione. Cyclic voltammogram tests, galvanostatic charge/discharge tests and electrochemical impedance spectra measurements were conducted for the study of electrochemical performance.

## 3 Results and discussion

The overall crystal structure and phase purity of the products were confirmed by the X-ray diffraction (XRD) spectrometry, as shown in Fig. 2. All the diffraction peaks are in good agreement with standard XRD patterns of rhombohedral $\alpha$-$Fe_2O_3$ (ICDD-PDF 33−0664) and tetragonal $SnO_2$ (ICDD-PDF 41−1445). According to the full width at half maximum (FWHM) of each peak in Fig. 2, it can be calculated from the Scherrer formula that the crystalline size of $SnO_2$ is only about 3 nm, much smaller than that of $Fe_2O_3$ with crystalline size of 25 nm.

The morphologies of the as-prepared materials were examined by transmission electron microscopy (TEM). The diameter of $\alpha$-$Fe_2O_3$ nanoparticles ranges from 50 to 200 nm, as shown in Fig. 3(a). The high-resolution TEM image (Fig. 3(b)) taken from the individual $\alpha$-$Fe_2O_3$ nanoparticle shows clear lattice fringe with an interplanar spacing of 0.27 nm, which corresponds well to the lattice spacing of (104) plane for $\alpha$-$Fe_2O_3$ phase. It can be seen from Figs. 3(c) and (d) that $\alpha$-$Fe_2O_3$@$SnO_2$ has a kind of core-shell structure, with a shell (30 nm in thickness) of
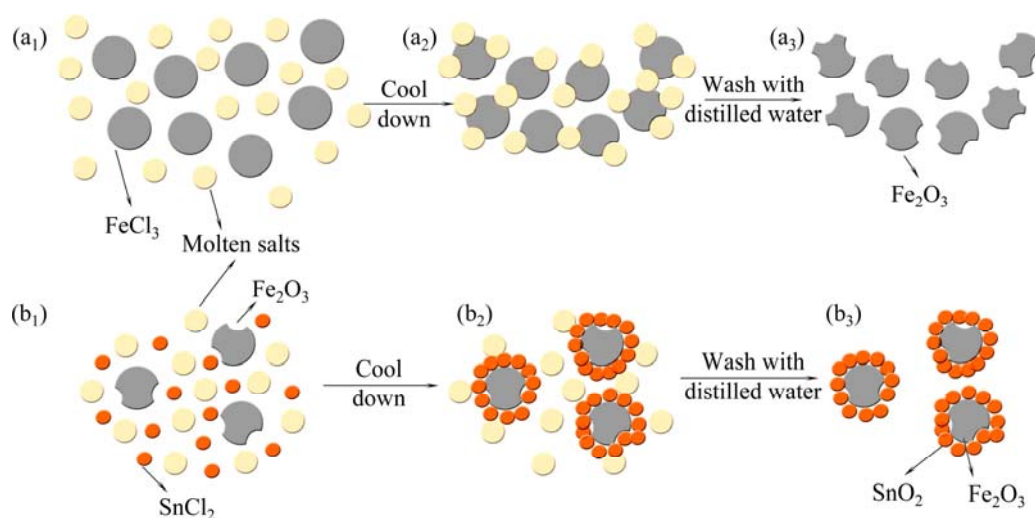


**Fig. 1** Schematic model for formation of different materials: ($a_1$) Mixture of raw materials; ($a_2$) Molten salts and $\alpha$-$Fe_2O_3$; ($a_3$) $\alpha$-$Fe_2O_3$; ($b_1$) Mixture of $\alpha$-$Fe_2O_3$, lithium salts and $SnCl_2$; ($b_2$) Molten salts, $SnO_2$ and $\alpha$-$Fe_2O_3$ particles; ($b_3$) $\alpha$-$Fe_2O_3$@$SnO_2$ nanocomposites
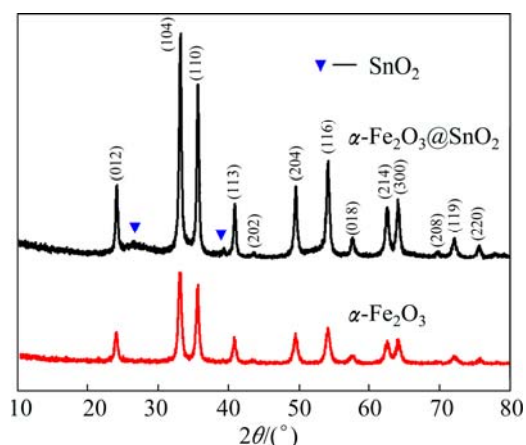
**Fig. 2** XRD patterns of $\alpha$-$Fe_2O_3$ nanoparticles and $\alpha$-$Fe_2O_3@$ $SnO_2$ nanocomposites

ultra-fine $SnO_2$ nanoparticles (about 5 nm in diameter) on the surface of $\alpha$-$Fe_2O_3$. Figure 3(d) shows the lattice spacings of $\alpha$-$Fe_2O_3$ (0.23 nm) and $SnO_2$ (0.33 nm), corresponding to the spacings of (006) and (110) planes, respectively.

The overall synthetic procedure and growth mechanism are described in Fig. 1. The molten salt method shows an accelerated reaction rate and controllable particle morphology, because the salt melt acts as a strong solvent and exhibits a high ionic diffusion rate [16]. $Fe_2O_3$ and $SnO_2$ may form with the oxidation of $Cl^-$ ions in the molten LiCl, and the oxidation of $Cl^-$ ions proceeds mainly by a reduction of oxygen in the air. Furthermore, the melted salts with their low melting point are helpful in hindering the growth of

$Fe_2O_3$ particles. When cooled down, the $Fe_2O_3$ particles were surrounded by the salts which were then washed away by de-ionized water, leaving pores behind, and thus generating nanoparticles. In the similar second step, the $Fe_2O_3$ particles act as nucleation sites to grow $SnO_2$ nanoparicles and futher form nanocoating $SnO_2$ layers.

The electrochemical performance of two samples was characterized systematically as anode material in LIBs. The cyclic voltammetry profiles (Fig. 4(a)) of the first charge/discharge cycle at a scanning rate of 0.1 mV/s exhibit three cathodic peaks of $\alpha$-$Fe_2O_3$ nanoparticles (1.6, 1.0 and 0.75 V), which correspond to the multiple phase transitions of hexagonal $\alpha$-$Li_xFe_2O_3$, $\alpha$-$Li_2Fe_2O_3$ and $Fe^0$, respectively. For the overall process, the first two reactions are barely reversible, while the last one is highly reversible for lithium storage [3,17]. Furthermore, four cathodic peaks of $\alpha$-$Fe_2O_3@SnO_2$ composites are observed at 1.55, 0.8, 0.6 and 0.2 V, and the first two peaks can be related to the formation of hexagonal $\alpha$-$Li_xFe_2O_3$ and $\alpha$-$Li_2Fe_2O_3$, respectively. The peak at 0.6 V may reveal two reactions, the complete reduction to $Fe^0$ and the reduction of $SnO_2$ to Sn, while the smallest peak at 0.2 V demonstrates the alloying of Sn with Li. A broad anodic peak located at 0.5−0.75 V corresponds to the de-alloying reaction of $Li_xSn$ [18−21].

Figures 4(b) and (c) display the first charge/ discharge curves and cycling performance of the products at a constant current density of 50 mA/g within a potential window of 0.01−3 V. The $\alpha$-$Fe_2O_3@SnO_2$ shows a remarkably improved initial discharge and charge capacity of 895 and 791 mA·h/g, respectively, which are almost twice of those of $\alpha$-$Fe_2O_3$ (571 and
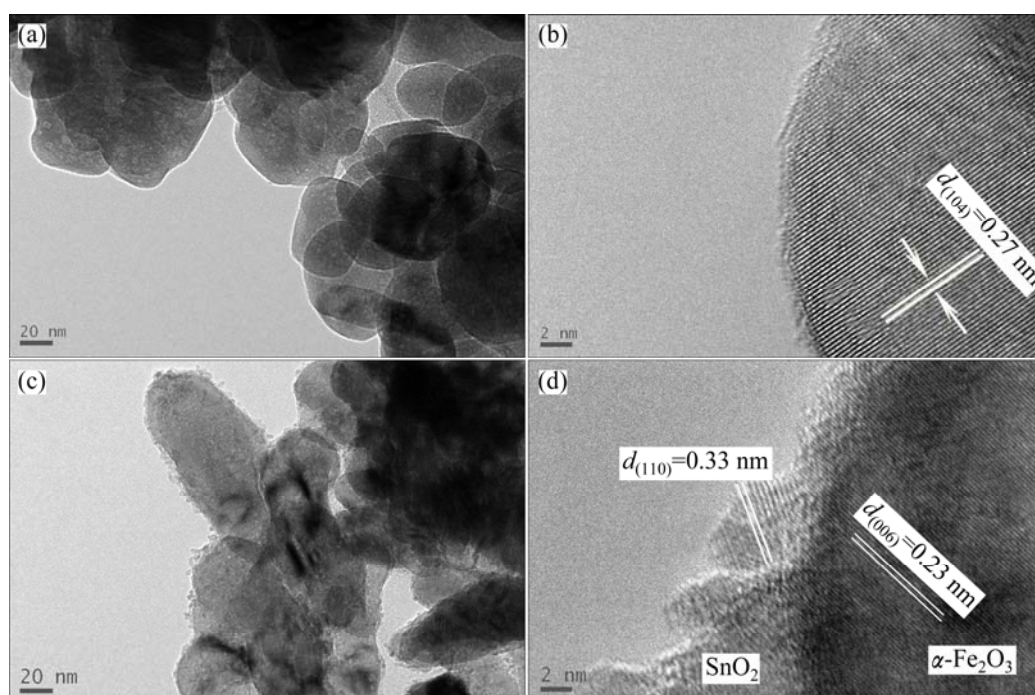


**Fig. 3** TEM images of pure $\alpha$-$Fe_2O_3$ nanoparticles (a, b) and $\alpha$-$Fe_2O_3@SnO_2$ nanocomposites (c, d)
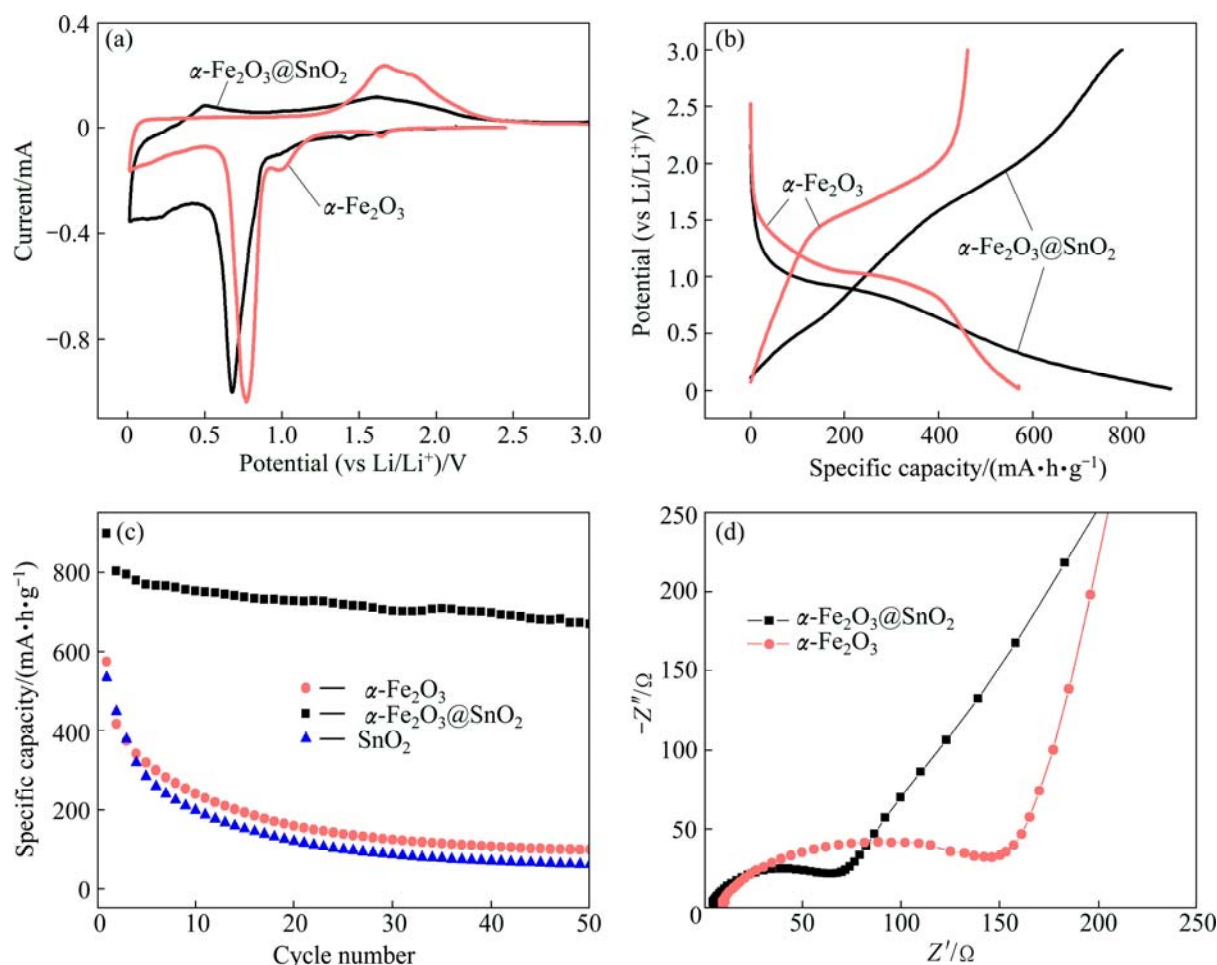
**Fig. 4** Electrochemical performance of two samples: (a) Cyclic voltammetry profiles; (b) First charge/discharge curves of electrodes at current density of 50 mA·h/g; (c) Cycling performance of two electrodes and pure $SnO_2$ electrode at current density of 50 mA·h/g; (d) Nyquist plots of samples

462 mA·h/g). After 50 cycles, it still has a discharge capacity of 664.8 mA·h/g which is very high compared with that of pure $\alpha$-$Fe_2O_3$ (97.5 mA·h/g) and pure $SnO_2$ (59.5 mA·h/g). The irreversible capacity loss of the first charge/discharge curves for $\alpha$-$Fe_2O_3$@$SnO_2$ may be mainly attributed to the irreversible processes such as inevitable formation of inorganic solid electrolyte interface (SEI) film and electrolyte decomposition, which are common to many anode materials [2,22−24].

Furthermore, electrochemical impedance spectroscopy measurements were performed, as shown in Fig. 4(d). Both curves exhibit a semicircle in high frequency region showing the charge transfer resistance of electrode and a straight line in low frequency region revealing the diffusion of lithium ions in the anode material. Compared with the numerical value of the semicircles, the charge transfer resistance of the $\alpha$-$Fe_2O_3$@$SnO_2$ electrode (75 Ω) is much smaller than that of the $\alpha$-$Fe_2O_3$ electrode (150 Ω). Smaller ohmic resistance of $\alpha$-$Fe_2O_3$@$SnO_2$ electrode means better electrical conductivity, which could be contributed to the

improved electrochemical cycling performance.

The $\alpha$-$Fe_2O_3$@$SnO_2$ core-shell nanoparticle electrode was also used to investigate the rate capability due to its superior cycling performance. The rate capabilities of the pure $\alpha$-$Fe_2O_3$ nanoparticle and $\alpha$-$Fe_2O_3$@$SnO_2$ nanocomposite electrodes were tested in the voltage window of 0.01−3.0 V at 50, 100, 200, 400, 1000, 2000 and 50 mA/g for 10 cycles each, as shown in Fig. 5. For the bare $\alpha$-$Fe_2O_3$ nanoparticle electrode, it shows specific capacity of 18 mA·h/g at 2000 mA/g, which is 3% of the initial specific capacity of 573 mA·h/g at 50 mA/g. While for the $\alpha$-$Fe_2O_3$@$SnO_2$ core-shell nanoparticle electrode, it shows specific capacities of 569, 528 and 493 mA·h/g at 400, 1000 and 2000 mA/g, respectively. The specific capacity of 493 mA·h/g at 2000 mA/g is up to 55% of the initial specific capacity of 898 mA·h/g at 50 mA/g. The results indicate that $SnO_2$ should have higher lithium diffusivity and electric conductivity than $\alpha$-$Fe_2O_3$. Such ultrathin $SnO_2$ nanocoating layer enhances the rate capability of the $\alpha$-$Fe_2O_3$@$SnO_2$ core-shell nanoparticle electrode.
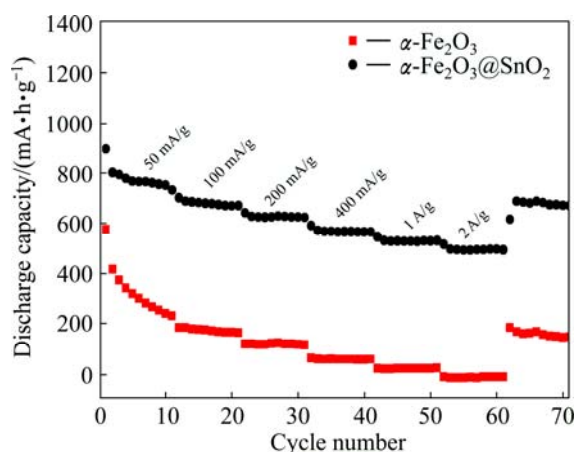
**Fig. 5** Rate properties of $\alpha$-Fe$_2$O$_3$ and $\alpha$-Fe$_2$O$_3$@SnO$_2$

## 4 Conclusions

1) A novel and effective carbon-free nanocoating strategy was developed for the synthesis of ultra-fine SnO$_2$ coating $\alpha$-Fe$_2$O$_3$ core-shell nanoparticles. This strategy only involves a two-step molten salt reaction at low temperature of 300 °C.

2) The as-prepared $\alpha$-Fe$_2$O$_3$@SnO$_2$ core-shell nanoparticles show enhanced specific capacity and better electrical conductivity than the bare $\alpha$-Fe$_2$O$_3$ nanoparticles.

3) This involved metal oxide nanocoating method is easy to be performed and scaled up, and the heat treatment temperature of 300 °C is much lower than that of other traditional solid-state annealing method and many carbon or other metal oxide nanocoating methods.

## References

[1]    ZHAO L, HU Y S, LI H, WANG Z X, CHEN L Q. Porous Li$_4$Ti$_5$O$_{12}$ coated with N-doped carbon from ionic liquids for Li-ion batteries [J]. Advanced Materials, 2011, 23: 1385−1388.

[2]    LIU J, TANG S S, LU Y K, CAI G M, LIANG S Q, WANG W J. Synthesis of Mo$_2$N nanolayer coated MoO$_2$ hollow nanostructures as high-performance anode materials for lithium-ion batteries [J]. Energy & Environmental Science, 2013, 6: 2691−2697.

[3]    YANG Q, LIANG Q, LIU J, LIANG S Q, TANG S S, LU P J, LU Y K. Ultrafine MoO$_2$ nanoparticles grown on graphene sheets as anode materials for lithium-ion batteries [J]. Materials Letters, 2014, 127: 32−35.

[4]    GUO Z P, DU G D. Ultra-fine porous SnO$_2$ nanopowder prepared via a molten salt process: A highly efficient anode material for lithium-ion batteries [J]. Journal of Materials Chemistry, 2009, 19: 3253−3257.

[5]    HAN F, LI D,  LI W C, LEI C, SUN Q, LU A H. Nanoengineered polypyrrole-coated Fe$_2$O$_3$@C multifunctional composites with an improved cycle stability as lithium-ion anodes [J]. Advanced Functional Materials, 2013, 23: 1692−1700.

[6]    ZHANG X, LIU H, PETNIKOTAD S, RAMAKRISHNAB S, FAN H J. Electrospun Fe$_2$O$_3$−carbon composite nanofibers as durable anode materials for lithium ion batteries [J]. Journal of Materials Chemistry A, 2014, 2: 10835−10841.

[7]    LI H, WANG Z X, CHEN L Q, HUANG X J. Research on advanced materials for Li-ion batteries [J]. Advanced Materials, 2009, 21: 4593−4607.

[8]    WANG Y Q, GU L, GUO Y G, LI H, HE X Q. TSUKIMOTO S. Rutile-TiO$_2$ nanocoating for a high-rate Li$_4$Ti$_5$O$_{12}$ anode of a lithium-ion battery [J]. Journal of the American Chemical Society, 2012, 134(18): 7874−7879.

[9]    LU J, QI D, DENG C, ZHANG X, YANG P. Controlled growth of SnO$_2$@Fe$_2$O$_3$ double-sided nanocombs as anodes for lithium-ion batteries [J]. Nanoscale, 2010, 2: 1892−1900.

[10]   LIU J, CHEN X L, WANG W J, SONG B, HUANG Q S. Secondary facet-selective nucleation and growth: Highly oriented straight SnO$_2$ nanowire arrays on primary micro-rods [J]. Crystal Growth & Design, 2009, 9: 1757−1761.

[11]   ZHU J X, YIN Z Y, YANG D, SUN T, YU H, HOSTER H E, HNG H H, ZHANG H, YAN Q Y. Hierarchical hollow spheres composed of ultrathin Fe$_2$O$_3$ nanosheets for lithium storage and photocatalytic water oxidation [J]. Energy & Environmental Science, 2013, 6: 987−993.

[12]   ZHANG D F, SUN L D, JIA C J, YAN Z G, YOU L P, YAN C H. Hierarchical assembly of SnO$_2$ nanorod arrays on $\alpha$-Fe$_2$O$_3$ nanotubes: A case of interfacial lattice compatibility [J]. Journal of the American Chemical Society, 2005, 127(39): 13492−13493.

[13]   WANG Y L, XU J J, WU H, XU M, PENG Z, ZHENG G F. Hierarchical SnO$_2$–Fe$_2$O$_3$ heterostructures as lithium-ion battery anodes [J]. Journal of Materials Chemistry, 2012, 22: 21923−21927.

[14]   LI Y F, HU Y J, JIANG H, HOU X Y, LI C Z. Phase-segregation induced growth of core–shell $\alpha$-Fe$_2$O$_3$/SnO$_2$heterostructures for lithium-ion battery [J]. Cryst Eng Comm, 2013, 15(34): 6715−6721.

[15]   ZHOU W, CHENG C, LIU J, TAY Y Y, JIANG J, JIA X. Epitaxial growth of branched $\alpha$-Fe$_2$O$_3$/SnO$_2$ nano-heterostructures with improved lithium-ion battery performance [J]. Advanced Functional Materials, 2011, 21: 2439−2445.

[16]   TANG W P, YANG X J, LIU Z H, KASAISHI S J, OOI K. Preparation of fine single crystals of spinel-type lithium manganese oxide by LiCl flux method for rechargeable lithium batteries. Part 1: LiMn$_2$O$_4$ [J] Journal of Materials Chemistry, 2002, 12: 2991−2997.

[17]   WANG Z, LUAN D, MADHAVI S, HU Y, LOU X W. Assembling carbon-coated $\alpha$-Fe$_2$O$_3$ hollow nanohorns on the CNT backbone for superior lithium storage capability [J]. Energy & Environmental Science, 2012, 5: 5252−5256.

[18]   LIAN P, LIANG S, ZHU X, YANG W, WANG H. A novel Fe$_3$O$_4$−SnO$_2$−graphene ternary nanocomposite as an anode material for lithium-ion batteries [J]. Electrochim Acta, 2011, 58: 81−88.

[19]   YU Y, CHEN C H, SHI Y. A tin-based amorphous oxide composite with a porous, spherical, multideck-cage morphology as a highly reversible anode material for lithium ion batteries [J]. Advanced Materials, 2007, 19: 993−997.

[20]   LU P J, LEI M, LIU J. Graphene nanosheets encapsulated alpha-MoO$_3$ nanoribbons with ultrahigh lithium ion storage properties [J]. Cryst Eng Comm, 2014, 16(29): 6745−6755.

[21]   QIN M L, LIU J, LIANG S Q, ZHANG Q, LI X L, LIU Y, LIN M Y. Facile synthesis of multiwalled carbon nanotube-V$_2$O$_5$ nanocomposites as cathode materials for Li-ion batteries [J]. Journal of Solid State Electrochemistry, 2014, 18(10): 2841−2846.

[22]   LUO Yun-ze, HE Li-hua, LIU Xu-heng. Effect of Mg doping on electrochemical performance of Li$_3$V$_2$(PO$_4$)$_3$/C cathode material for

lithium ion batteries [J]. Transactions of Nonferrous Metals Society of China, 2015, 25(7): 2266−2271.

[23] YIN Wu-mei, ZHANG Ting-ting, ZHU Qing, CHEN Quan-qi, LI Gu-cai, ZHANG Ling-zhi. Synthesis and electrochemical performance of Li$_{3−2x}$Mg$_x$V$_2$(PO$_4$)$_3$/C composite cathode materials for lithium-ion batteries [J]. Transactions of Nonferrous Metals Society of China, 2015, 25(6): 1978−1985.

[24] HUANG Yue, WANG Zhi-xing, LI Xin-hai, GUO Hua-jun, WANG Jie-xi. Synthesis of Ni$_{0.8}$Co$_{0.1}$Mn$_{0.1}$(OH)$_2$ precursor and electrochemical performance of LiNi$_{0.8}$Co$_{0.1}$Mn$_{0.1}$O$_2$ cathode material for lithium batteries [J]. Transactions of Nonferrous Metals Society of China, 2015, 25(7): 2253−2259.

# 低温熔盐法制备 $\alpha$-Fe$_2$O$_3$@SnO$_2$ 核壳结构纳米颗粒

刘 刚 [1,2]，孙维佳 [2]，唐莎莎 [3]，梁叔全 [3]，刘 军 [3]

1. 中南大学 湘雅医院肝胆肠外科研究中心，长沙 410008；
2. 中南大学 湘雅医院普外科，长沙 410008；
3. 中南大学 材料科学与工程学院，长沙 410083

**摘　要**：采用一种经济有效的非碳纳米包覆技术制备超细 SnO$_2$ 颗粒包覆 $\alpha$-Fe$_2$O$_3$ 核壳形式的纳米结构材料。这种技术仅涉及两步低温(300 °C)熔盐反应。相对于纯的 $\alpha$-Fe$_2$O$_3$ 纳米颗粒，所制备的 $\alpha$-Fe$_2$O$_3$@SnO$_2$ 纳米核壳颗粒显示出更好的电化学性能。金属氧化物纳米包覆的方法比较容易实施，其热处理温度远低于传统的固相烧结反应和其他碳或金属氧化物纳米包覆方法的热处理温度。这种新的熔盐反应包覆技术也可用于制备其他氧化物纳米包覆结构，并可将这些纳米复合结构材料用于锂离子电池电极材料。

**关键词**：纳米材料；锂离子电池；熔盐反应；能源材料；纳米包覆

**(Edited by Mu-lan QIN)**